Available online at www.sciencedirect.com
ScienceDirect
Journal of Power Sources 175 (2008) 383–389
JOURNAL OF POWER SOURCES
www.elsevier.com/locate/jpowsour

Evaluation of activated carbon adsorbent for fuel cell cathode air filtration

Xiaowei Ma [a,c], Daijun Yang [a,b], Wei Zhou [a,b], Cunman Zhang [a,b], Xiangmin Pan [a,b], Lin Xu [c], Minzhong Wu [c], Jianxin Ma [a,b,*]

[a] *School of Automotive Studies, Tongji University, Shanghai 201804, PR China*
[b] *Clean Energy Automotive Engineering Center, Tongji University, Shanghai 201804, PR China*
[c] *Shanghai Fuel Cell Vehicle Powertrain Co. Ltd., Shanghai 201804, PR China*

Received 20 July 2007; received in revised form 31 August 2007; accepted 31 August 2007
Available online 19 September 2007

Abstract

The effectiveness of a commercial activated carbon modified by KOH (KMAC) was evaluated as adsorbent for purifying NO_x and SO_2, which are the major contaminants in fuel cell cathode air stream. The N_2 adsorption–desorption isotherms of KMAC samples showed that the surface structure of the activated carbon was changed significantly by KOH impregnation. The sample of KMAC with a loading of 10.1% KOH by weight presented the highest adsorption capacities for both NO_x and SO_2, which were 96 mg g^{-1} and 255 mg g^{-1}, respectively. A pre-exposure of KMAC to CO_2 caused neither effect on the adsorption of NO_x nor on the adsorption of SO_2. KMAC could fully protect a 250 W proton exchange membrane fuel cell (PEMFC) stack from 1100 ppb of NO_x and 250 ppb of SO_2 for about 130 h.

Keywords: Activated carbon; KOH modification; Adsorption; PEMFC; Air filtration; Air contaminants

1. Introduction

Proton exchange membrane fuel cells (PEMFCs) are being developed as an alternative to the internal combustion engine (ICE) for automotive propulsion in order to reduce fossil fuel consumption. One potential problem with PEMFCs however is that the cathode catalyst could be poisoned by air contaminants, especially once emitted from ICE vehicles. There have been many studies regarding the impact of various air contaminants [1–5]. For example, 1 ppm of NO_2 could reduce fuel cell performance by 10% while the same concentration of SO_2 caused a 35% loss of cell voltage within 100 h [1]. Hundred and forty parts per million of NO_x ($NO:NO_2 = 9:1$) could cause a 30% reduction in cell voltage within 5 min [2]. However, the effects of CO and hydrocarbon (i.e. benzene and propane) were less severe than those of NO_x and SO_2 [4,5]. Furthermore, the performance of fuel cells could not be fully recovered after poisoning by NO_x or SO_2. Therefore, it is a challenge to prevent the cathode from the contamination of NO_x and SO_2 in air when operating fuel cell vehicles in real environment. To date, few studies have addressed the critical problem of protecting PEMFCs from air contamination.

There are two options for dealing with air contamination of fuel cells: improvement of catalyst durability and chemical adsorption. The latter option can be incorporated into a filter system, forming an adsorptive filter. The designing parameters of an adsorptive filter, including saturation capacity, removal efficiency and pressure drop, depend on the inlet air properties (contaminants, concentration and air flow rate), filter design options (packed bed or microfibrous material) and filter footprint (area, thickness and weight) [6]. Obviously, the selection and evaluation of adsorbent are key issues for the adsorptive filter designing.

One effective selection for the adsorbent is activated carbons (ACs), which are a well-known high porous and low cost

* Corresponding author at: School of Automotive Studies, Tongji University, Shanghai 201804, PR China. Tel.: +86 21 69589480; fax: +86 21 69589355.
E-mail address: jxma@mail.tongji.edu.cn (J. Ma).

0378-7753/$ – see front matter © 2007 Elsevier B.V. All rights reserved.
doi:10.1016/j.jpowsour.2007.08.116

material. Many studies have investigated the removal of NO_x and SO_2 by using ACs. It was reported that NO_x and SO_2 adsorption capacities are related not only to the surface properties of ACs, but also to the modification process [7–10]. In addition, adsorption temperature, surface oxygen functional groups, space velocity and adsorption pressure could affect the adsorption of NO_x or SO_2 to some extent [11–13]. However, most of these studies did not focus on the application in fuel cells. On the other hand, the co-existence of CO_2 on the adsorption of NO_x and SO_2 was not investigated, though a high CO_2 adsorption capacity on modified activated carbon (MAC) was reported [14].

In the present work, a series of KMAC samples were prepared by impregnating activated carbon into potassium hydroxide solutions at different concentrations. The KMAC samples were characterized by N_2 adsorption–desorption isotherms and their behaviors for the adsorption of NO_x and SO_2 were studied. In addition, the efficiency of KMAC as fuel cell air filter material was evaluated by connecting a KMAC filled fixed bed reactor to a 250 W fuel cell stack.

2. Experimental

2.1. Adsorbent preparation

Four types of commercial activated carbon samples were compared in order to select a suitable type with better surface and pore structure. Listed in Table 1 are their textural properties, measured by BET method (ASAP 2020, Micrometrics). The BET surface area (S_B) and total pore volume (V_T) of AC-1 are much higher than those of others, but its micropore area (S_M) is slightly lower than those of AC-2 and AC-4. This suggests that more mesopores and macropores exist in the AC-1 sample. According to Claudino et al. [11] and Neathery et al. [15], the adsorption capacities of ACs do not mainly depend on the micropore area. Furthermore, it is easier for the mesopores and macropores to accommodate potassium deposited on the activated carbon surface. Therefore, AC-1 (hereinafter denoted by AC) has been considered to be the best one for KOH modification and further experiments.

To remove possibly contained volatiles, AC was first calcined in a furnace under helium atmosphere at 800 °C for 1 h. It was then impregnated into KOH solutions at different concentrations between 0.1 M and 1 M with stirring at 45 °C for 3 h, followed by dehydration at 100 °C for 8 h in a vacuum oven. Next, the modified samples were activated at 600 °C for 1 h with a constant heating rate of 10 °C min^{-1} in He. Finally, five adsorbent samples (AC and KMACs) were prepared and kept in a desiccator to avoid moisture and contaminants. The KOH loading weights and textural characteristics of all five samples are shown in Table 2.

Table 1
Textural properties of commercial activated carbon samples

Samples	BET surface areas, S_B ($m^2\ g^{-1}$)	Micropore areas, S_M ($m^2\ g^{-1}$)	S_M/S_B	Total pore volume, V_T ($cm^3\ g^{-1}$)	Average pore width (nm)
AC-1	1716.33	492.97	0.29	1.01	2.35
AC-2	905.21	646.64	0.71	0.44	1.93
AC-3	442.19	421.67	0.95	0.20	1.85
AC-4	840.76	588.50	0.70	0.48	2.26

2.2. Adsorption procedure

The prepared adsorbent was filled in a fixed bed reactor (see Fig. 1). Eight thousand parts per million of NO_x/N_2 ($NO:NO_2 = 9:1$) and 7500 ppm of SO_2/N_2 were fed to the reactor. The flow rates were controlled by mass flow meters (Alicat) and the concentrations of NO_x and SO_2 were monitored and analysed by a MS gas analyser (IMSQ4-GP, ABB). The adsorption experiments were operated at ambient temperature at about 25 °C.

2.3. PEMFC stack testing

The effect of adsorbent on the performance of fuel cell was investigated on a 250 W PEMFC stack. The fixed bed reactor filled with KMAC-3 was used and connected to the cathode inlet of the stack. A simulated air contaminated with 1100 ppb of NO_x ($NO:NO_2 = 9:1$) and 250 ppb SO_2 was fed into the reactor and then to the stack (see Fig. 1). The air stream could also be skipped over the reactor and fed directly into the stack. The H_2 (99.999%) on the anode was humidified and the operating temperature of the stack was set at 70 °C.

2.4. Calculation of adsorption

The adsorption capacities and efficiencies of both NO_x and SO_2 on activated carbon adsorbents can be calculated according to the following equations.

Theoretically, the effective adsorption time (T_s) is related to equilibrium adsorption volume (Q), interstitial velocity (u), inlet volume concentration (C_0), adsorption efficiency (η) and

Table 2
KOH loading and textural characteristics of adsorbent samples

Samples	KOH loading (wt.%)	S_B ($m^2\ g^{-1}$)	S_M ($m^2\ g^{-1}$)	S_M/S_B	V_T ($cm^3\ g^{-1}$)	Average pore width (nm)
AC	0	1716.33	492.97	0.29	1.01	2.35
KMAC-1	2.2	1474.40	438.73	0.30	0.86	2.34
KMAC-2	5.3	1342.27	413.59	0.31	0.78	2.34
KMAC-3	10.1	1153.36	337.19	0.29	0.68	2.35
KMAC-4	18.3	626.13	193.93	0.31	0.37	2.38

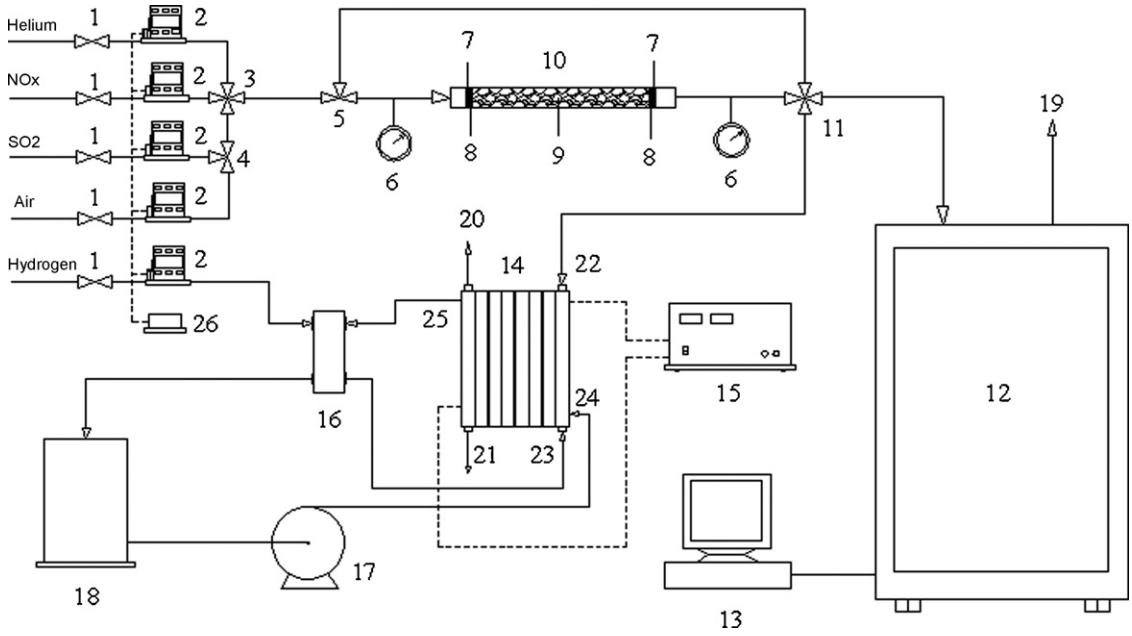

Fig. 1. Schematic diagram of experimental set-up. 1, two-way valve; 2, mass flow meter (MFM); 3 and 11, four-way valve; 4 and 5, three-way valve; 6, manometer; 7, stainless steel mesh; 8, asbestos; 9, adsorbent; 10, fixed bed reactor; 12, MS gas analyser; 13, computer; 14, PEMFC stack; 15, electronic load; 16, humidifier; 17, pump; 18, water tank; 19, MS analyser outlet; 20, H_2 outlet; 21, air outlet; 22, air inlet; 23, H_2 inlet; 24, water inlet; 25, water outlet; 26, MFM control unity.

cross-section area of the fixed bed reactor (A):

$$T_s = \frac{Q}{uC_0\eta A} \tag{1}$$

where $u = v/\varepsilon$ (v is the superficial velocity of NO_x or SO_2 and ε is the total porosity of adsorbent). T_s can be obtained directly from the adsorption experiment. However, because a genuine adsorption equilibrium is difficult to reach, T_s is defined in this paper as the interval between adsorption beginning and the time when the outlet concentration (C) of NO_x or SO_2 recovers to 95% of C_0.

The equivalent breakthrough time (T^*) is proposed based on the assumption, in which the concentration of NO_x or SO_2 increases to its initial value immediately as breakthrough occurs. Therefore, T^* can be calculated according to the following equation:

$$T^* = \int_0^{T_s} \left(\frac{C_0 - C}{C_0}\right) \mathrm{d}t \tag{2}$$

Based on Eq. (1), the calculation of adsorption efficiency can be expressed as

$$\eta = \frac{\int_0^{T_s}(C_0 - C)\mathrm{d}t}{\int_0^{T_s} C_0\,\mathrm{d}t} \tag{3}$$

Furthermore, the adsorption weight (Q_a) can be calculated according to the following equation:

$$Q_a = \frac{C_0 T^* q_0 M}{22.4w} \tag{4}$$

where q_0 is the flow rate of gas mixture, M the molecular weight of NO_x or SO_2 and w is the adsorbent weight.

3. Results and discussion

3.1. Porosity characterization

Fig. 2 shows N_2 adsorption–desorption isotherms for all samples at −196 °C. The isotherms behaved a form of type IV with a hysteresis loop, indicating the presence of mesopores. The hysteresis loop in each isotherm occurred at a relative pressure of approximately 0.4. Therefore, capillary condensation could start from the pore size of 3 nm [16]. As seen in Fig. 2, N_2 adsorption capacity of KMAC decreased evidently with an increase in KOH content. This suggests that the physical structure of activated carbon was apparently changed by KOH modification. More detailed textural results of the samples are given in Table 2. A significant decrease in S_B and V_T

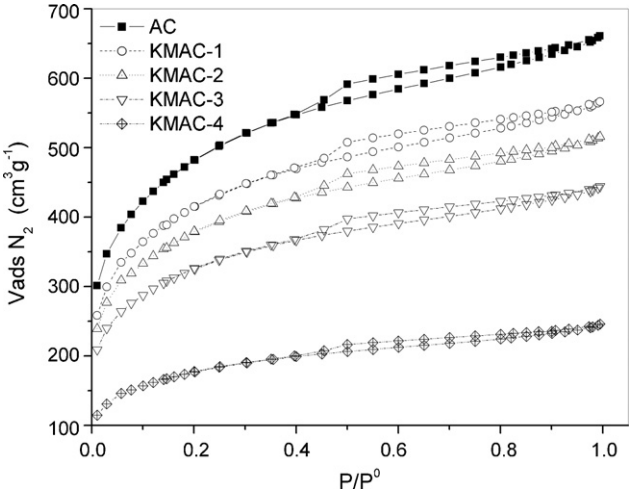

Fig. 2. N_2 adsorption–desorption isotherms for AC and KMACs.

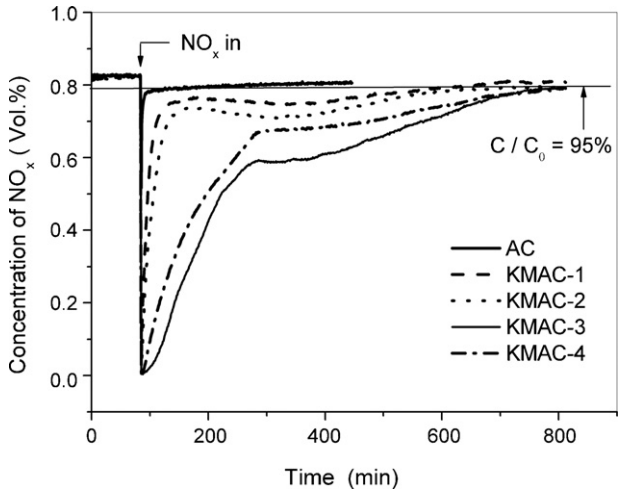

Fig. 3. Effects of KOH modification on NO_x (NO:NO_2 = 9:1) adsorption (adsorption temperature = 25 °C; flow rate = 60 mL min^{-1}; bed depth = 3 cm).

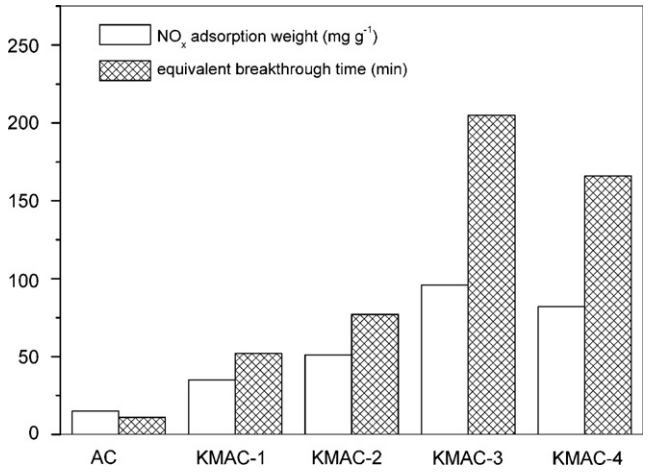

Fig. 4. NO_x adsorption weights and equivalent breakthrough times on AC and KMACs.

could be found when the loading of KOH in KMAC samples was high. The relationship between S_M and KOH loading showed a similar tendency as S_B and V_T, and the ratios of S_M to S_B were almost constantly at 0.3. It seems that along with micropores, mesopores and macropores were also influenced by KOH modification.

3.2. NO_x and SO_2 adsorption

Fig. 3 shows the breakthrough curves of NO_x adsorption on AC and KMACs. In order to accelerate the adsorption, a high concentration of NO_x was used in screening the adsorbents. It is evident that the NO_x adsorption profiles behaved differently. On the breakthrough curve of AC, the concentration of NO_x recovered soon from a complete adsorption to a level at about 95% of the inlet concentration (C_0), showing only a small amount of NO_x was captured by AC. On the breakthrough curves of KMAC-1 and KMAC-2, the recovery to a relatively stable value occurred at about 175 min and they took a longer time for about 600 min to reach a concentration level of 95% of C_0. In addition, there existed a fluctuation on the curves, which may be caused by the oxidation of NO to NO_2 and the additional adsorption of NO_2 [13,17,18]. Since there was no O_2 in the gas mixture, the conversion between NO and NO_2 might be promoted by the surface oxygen species, provided by oxygen functional groups in KMACs. The samples of KMAC-3 and KMAC-4 showed a longer breakthrough time for the adsorption of NO_x. In this case, the concentration of NO_x was recovered to 95% of C_0 after about 800 min.

According to Eqs. (2) and (4), the equivalent breakthrough time (T^*) and NO_x adsorption weight (Q_a) of the samples were calculated and the results are shown in Fig. 4. It can be seen that both T^* and Q_a increased with KOH loading and reached the maximum on the sample KMAC-3 with a KOH loading of 10.1%. The NO_x adsorption weight on KMAC-3 was 96 mg g^{-1}, which is 6.4 times of that of AC. Obviously, the modification of KOH enhanced the NO_x adsorption capacity of activated carbon very significantly. However, when KOH loading exceeded 10.1%, as in the case of KMAC-4, the NO_x adsorption capacity decreased. One of the reasons could be that some pores in AC might be blocked by KOH deposition and aggregation. The data of S_B and V_T of KMAC-4 in Table 2, which decreased significantly, provided additional evidence. Therefore, S_B and V_T could be the surface fingerprint of KMAC for NO_x adsorption capacity and should be controlled moderately during KOH modification.

The breakthrough curves of SO_2 adsorption on AC and KMACs are plotted in Fig. 5. In comparison to the breakthrough of NO_x, the breakthrough of SO_2 took place more slowly. For instance, the breakthrough of SO_2 on AC started at 50 min after the introduction of SO_2 and the start point of breakthrough for the KMAC samples needed much longer time. However, it was easier for the breakthrough of SO_2 to reach a concentration level of 95% of C_0 than that in the case of NO_x. It is well known that the acidity of SO_2 is higher than that of NO_x. Therefore, the interaction between SO_2 and KMAC would be stronger and the adsorption of SO_2 became easier than that of NO_x.

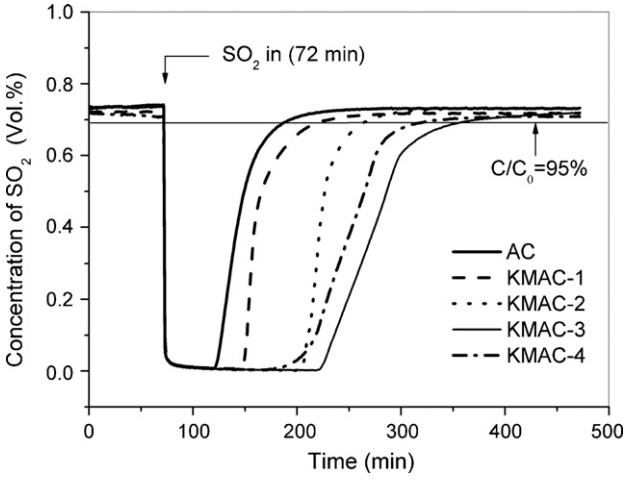

Fig. 5. Effects of KOH modification on SO_2 adsorption (adsorption temperature = 25 °C; flow rate = 60 mL min^{-1}; bed depth = 3 cm).

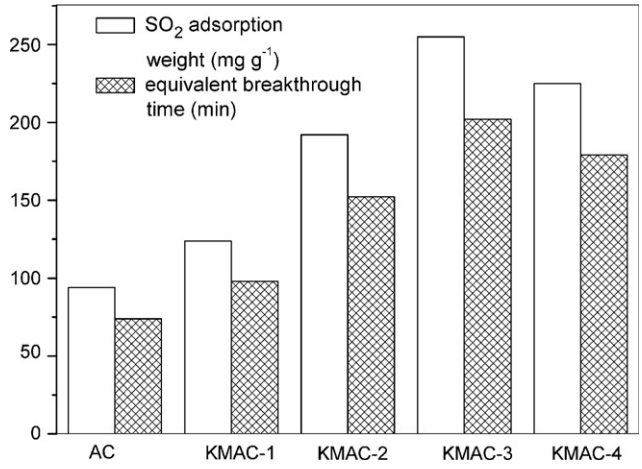

Fig. 6. SO_2 adsorption weights and equivalent breakthrough times on AC and KMACs.

The calculated T^* and Q_a of SO_2 for all samples are shown in Fig. 6. The effects of KOH loading on T^* and Q_a of SO_2 adsorption are similar to those of NO_x. Of all the samples, KMAC-3 had the best performance for SO_2 adsorption. The Q_a of SO_2 on KMAC-3 was 255 mg g^{-1}, which is 2.7 times of that of AC. Therefore, KMAC-3 was recognized as the most effective adsorbent and adopted in the subsequent experiments.

3.3. Effect of CO_2

Usually, air contains about 350 ppm of CO_2. Since CO_2 is acidic in nature, its co-existence may affect the adsorption of NO_x and SO_2. In order to reveal the effect of CO_2, the adsorbent KMAC-3 was exposed to air for 24 h to establish a saturated state of CO_2 adsorption. Then, the breakthrough behaviors of NO_x and SO_2 on the CO_2 pre-treated sample were investigated. The results are shown in Fig. 7.

Fig. 7a shows the effect of CO_2 on the breakthrough of NO_x. It can be seen that a desorption of CO_2 took place as soon as NO_x was introduced into the adsorption reactor and a maximum of CO_2 occurred at the time of 135 min. The desorption of CO_2 was stopped at the time of about 300 min, where the breakthrough of NO_x turned into a flat stage. The phenomenon indicates that NO_x replaced the adsorbed CO_2 due to a stronger interaction with KMAC-3. Furthermore, it was found that the adsorption capacity, Q_a was almost the same as that without the co-existence of CO_2, providing the evidence of a complete replacement of CO_2 by NO_x.

The effect of CO_2 on the adsorption of SO_2 is shown in Fig. 7b. Obviously, a replacement of CO_2 by SO_2 occurred. However, unlike the adsorption of NO_x, the desorption of CO_2 was delayed for about 170 min. The possible explanation to the phenomenon is that SO_2 is a much more acidic gas and can find more sites on the adsorbent surface in addition to the sites occupied by CO_2. In comparison of the breakthrough curve in Fig. 7b to that of KMAC-3 in Fig. 5, it is evident that the adsorption capacity of SO_2 was not influenced by the co-existence of CO_2.

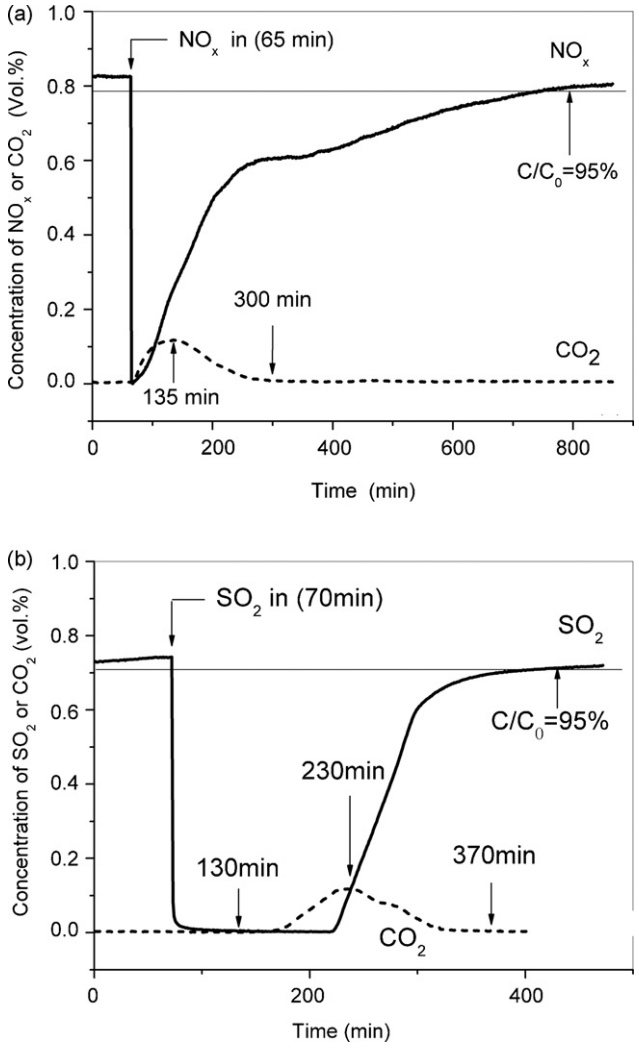

Fig. 7. Breakthrough curves of NO_x (a) and SO_2 (b) adsorption on KMAC-3 with CO_2 presence (adsorption temperature = 25 °C; flow rate = 60 mL min^{-1}; bed depth = 3 cm).

3.4. Pressure drop testing

Prior to the investigation of the feasibility of using KMAC-3 to protect PEMFC stack from NO_x and SO_2, pressure drop caused by KMAC-3 in the adsorbent reactor was tested at different inlet air pressure and flow rates. Fig. 8 shows the tested and calculated results according to the modified Ergun equations [19]. It can be found that the influence of inlet air pressure on the pressure drop was insignificant. However, it increased with the increase of air flow rate approximately linearly. The independence of pressure drop on the inlet pressure is due to less change of air viscosity in the range between 1.0 bar and 2.5 bar.

Fig. 9 shows the ratios of pressure drop to inlet air pressure (R_{pd}) of KMAC-3 at different air flow rates. It is clear that the higher the inlet air pressure, the lower the relative pressure drop will be. At the inlet pressure of 1.5 bar, the highest R_{pd} is about 2.5%. The influence of such level of pressure drop on the performance of a 250 W stack was investigated and will be discussed in the following section.

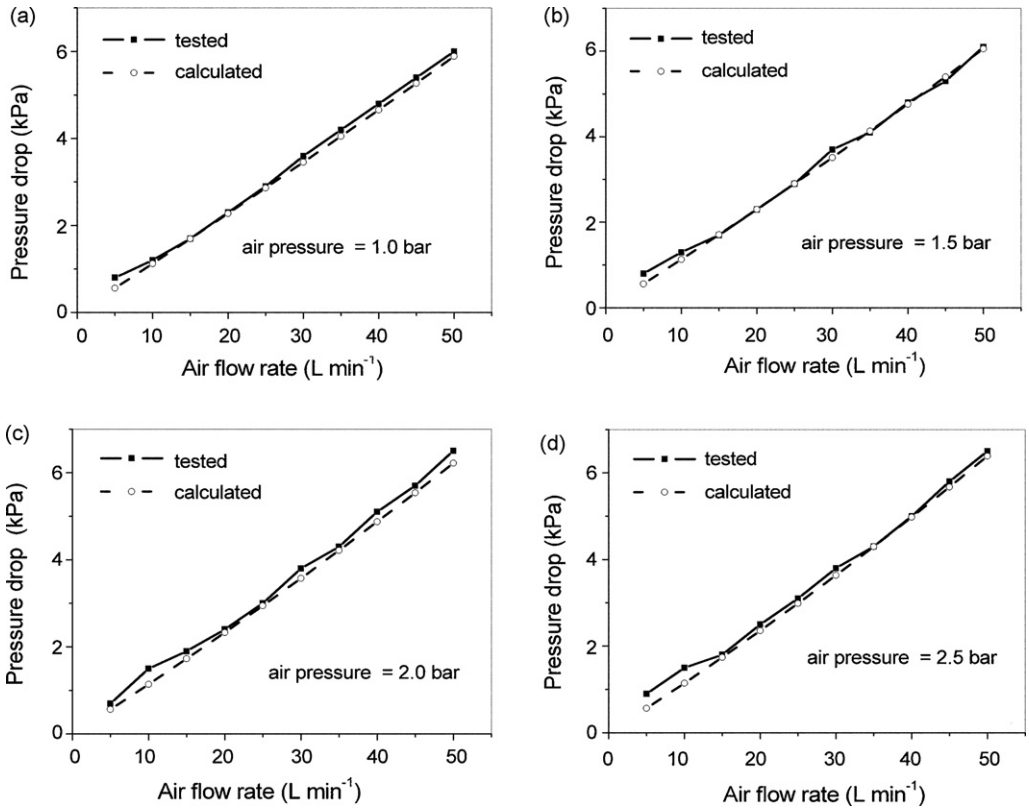

Fig. 8. Tested and calculated pressure drops of KMAC-3 in the fixed bed reactor (bed depth = 3 cm).

3.5. PEMFC stack testing

The application of KMAC-3 as an adsorptive filter material for protecting fuel cells was evaluated. The experiment was carried out on a 250 W PEMFC stack (see Fig. 1). The concentrations of NO_x ($NO:NO_2 = 9:1$) and SO_2 are 1100 ppb and 250 ppb, respectively. KMAC-3 was filled in the fixed bed reactor and connected to the cathode inlet of the stack. The inlet air pressure was set at 1.5 bar. The decrease of stack voltage caused by the pressure drop was only about 20 mV (see Fig. 10). Therefore, the effect of pressure drop resulted by the reactor was negligible.

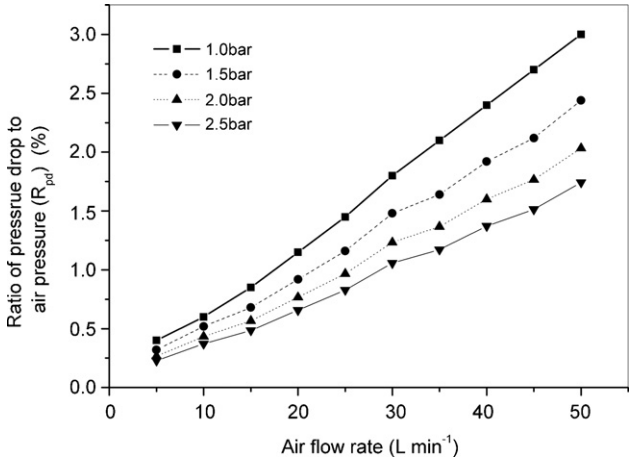

Fig. 9. Influences of air pressure and flow rates on pressure loss for KMAC-3 (bed depth = 3 cm).

Fig. 10 also shows the measurement of stack voltage when NO_x and SO_2 contaminated air was fed directly into the cathode of the stack. In neat air case, the stack voltage declines from 3.9 V to 3.7 V within 80 h and kept a steady state at about 3.65 V till the end of experiment. In contaminated air case, the voltage declined sharply from 3.9 V to about 2.7 V within 30 h. Thereafter, no further decrease in stack voltage was observed. Therefore, the presence of NO_x and SO_2 caused a damage of stack performance by 30.7% when no protesting measure was taken.

Fig. 11 shows the efficiency of KMAC-3 in protecting stack from the poisoning of NO_x and SO_2. In the first 130 h, the stack

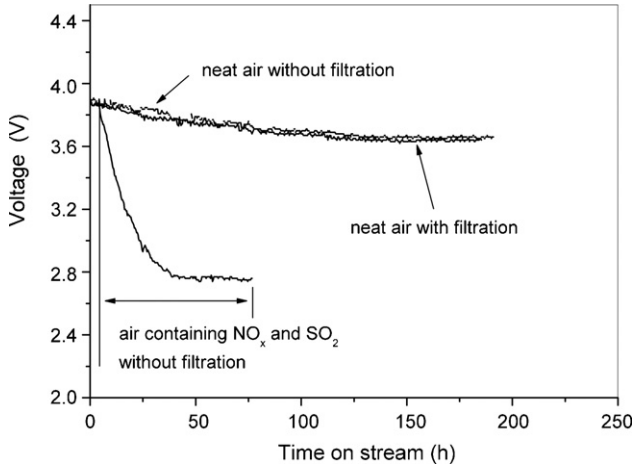

Fig. 10. Influences of NO_x, SO_2 and air pressure drop on stack performance (air pressure = 1.5 bar; bed depth = 3 cm; air flow rate = 30 L min^{-1}; current density = 280 mA cm^{-2}).

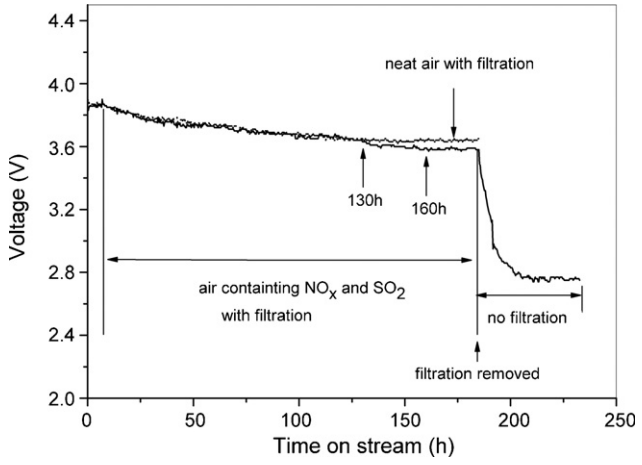

Fig. 11. *V–t* curves of 250 W stack with NO_x and SO_2 filtration (air pressure = 1.5 bar; bed depth = 3 cm; air flow rate = 30 L min^{-1}; current density = 280 mA cm^{-2}).

performance was the same as that under neat air, showing that the stack was not affected by the contaminants. During this period of time, the breakthrough of NO_x and SO_2 on KMAC-3 might not occur, because the concentrations of NO_x and SO_2 used in this experiment were much lower than those used in Figs. 3 and 5. In the second stage from 130 h to 160 h, the stack voltage declined slightly. The decrease was about 1.6%. At this stage, the breakthrough of NO_x and SO_2 might occur, though the desorption of NO_x and SO_2 was insignificant. After 160 h, the decline became flat. The same observation existed in Fig. 10, too. However, when the filtration was by-passed, i.e. NO_x and SO_2 were introduced again into the stack directly, the voltage dropped rapidly to about 2.7 V. Obviously, KMAC-3 was an efficient adsorbent and could be used in fuel cell air filter.

4. Conclusions

A commercial activated carbon modified by KOH was used to remove NO_x and SO_2 in air at ambient temperature (25 °C) and its potential application in fuel cell air filter was evaluated. The following conclusions can be drawn:

(1) The adsorption capacities of activated carbon for NO_x and SO_2 could be affected by surface structure and more significantly by KOH modification. Activated carbon loaded with 10.1% KOH by weight (sample KMAC-3) showed the best property and the adsorption weights for NO_x and SO_2 were 96 mg g^{-1} and 255 mg g^{-1}, respectively.
(2) The co-existence of CO_2 did not cause any effect on the adsorption of NO_x and SO_2 on KMAC-3.
(3) The pressure drop caused by air flowing through the adsorbent was about 2.5% at an inlet air pressure of 1.5 bar and led only to a decrease of 20 mV in voltage for a 250 W PEMFC stack.
(4) Directly feeding a contaminated air with 1100 ppb NO_x and 250 ppb SO_2 to the 250 W stack caused a decrease in voltage by 30.7%. When a reactor filled with KMAC-3 adsorbent was used before the stack, the performance of stack did not change any more within 130 h. Therefore, KMAC is a type of potential filter material for protecting PEMFC from the poisoning by NO_x and SO_2.

Acknowledgements

The authors appreciate Henkel Professorship at Tongji University and the International S&T Cooperation Program of Ministry of Science & Technology of China (Grant number 2004DFB01500) for financial support.

References

[1] F.N. Jing, M. Hou, W.Y. Shi, J. Fu, H.M. Yu, P.W. Ming, B.L. Yi, J. Power Sources 166 (2007) 172–176.
[2] D.J. Yang, J.X. Ma, L. Xu, M.Z. Wu, H.J. Wang, Electrochim. Acta 51 (2006) 4039–4044.
[3] R. Mohtadi, W.K. Lee, J.W.V. Zee, J. Power Sources 138 (2004) 216–225.
[4] M.C. Bétournay, G. Bonnell, E. Edwardson, D. Paktunc, A. Kaufman, A.T. Lomma, J. Power Sources 134 (2004) 80–87.
[5] J.M. Moore, P.L. Adcock, J.B. Lakeman, G.O. Mepsted, J. Power Sources 85 (2000) 254–260.
[6] D.M. Kennedy, D.R. Cahela, W.H. Zhu, K.C. Westrom, R.M. Nelms, B.J. Tatarchuk, J. Power Sources 168 (2007) 391–399.
[7] W.L. Young, W.P. Jee, J.J. Se, K.C. Dae, E.Y. Jae, Carbon 42 (2004) 59–69.
[8] J.H. Yun, D.K. Choi, Environ. Sci. Technol. 36 (2002) 4928–4935.
[9] Y.W. Lee, H.J. Kim, J.W. Park, B.U. Choi, D.K. Choi, J.W. Park, Carbon 41 (2003) 1881–1888.
[10] Y.W. Lee, D.K. Choi, J.W. Park, Carbon 40 (2002) 1409–1417.
[11] A. Claudino, J.L. Soares, R.F.P.M. Moreira, H.J. José, Carbon 42 (2004) 1483–1490.
[12] J.L. Zhu, Y.H. Wang, J.C. Zhang, R.Y. Ma, Energ. Convers. Manage. 46 (2005) 2173–2184.
[13] W.G. Klose, S. Rincon, Fuel 86 (2007) 203–209.
[14] A. Arenillas, F. Rubiera, J.B. Parra, C.O. Ania, J.J. Pis, Appl. Surf. Sci. 252 (2005) 619–624.
[15] J.K. Neathery, A.M. Rubel, J.M. Stencel, Carbon 35 (1997) 1321–1327.
[16] Y.C. Chiang, P.C. Chiang, E.E. Chang, Chemosphere 37 (1998) 237–247.
[17] I. Mochida, N. Shirahama, S. Kawano, Y. Korai, A. Yasutake, M. Tanoura, S. Fujii, M. Yoshikawa, Fuel 79 (2000) 1713–1723.
[18] J. Yang, G. Mest, D. Herein, R. Schloegl, J. Find, Carbon 38 (2000) 729–740.
[19] D.R. Cahela, B.J. Tatarchuk, Catal. Today 69 (2001) 33–39.